The human nuclear exosome targeting complex is loaded onto newly synthesized RNA to direct early ribonucleolysis

Article

Cell Reports

The Human Nuclear Exosome Targeting Complex Is Loaded onto Newly Synthesized RNA to Direct Early Ribonucleolysis

Graphical Abstract

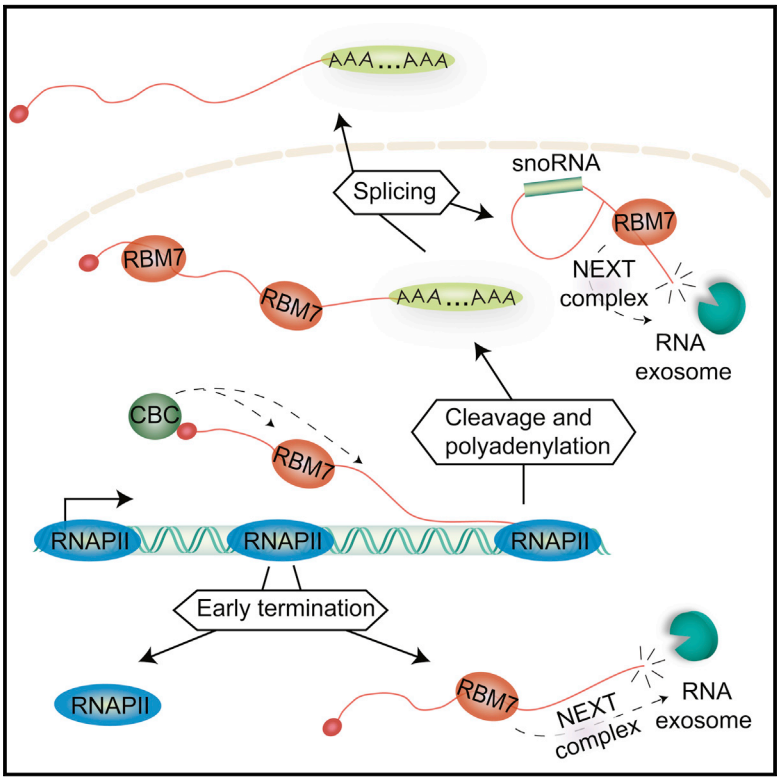

Authors

Michal Lubas, Peter Refsing Andersen, ..., Grzegorz Kudla, Torben Heick Jensen

Correspondence

thj@mb.au.dk

In Brief

The nuclear RNA exosome is directed to many of its nucleoplasmic substrates by the nuclear exosome targeting (NEXT) complex. Lubas et al. now use iCLIP to follow NEXT targeting to RNA via its RNA binding component RBM7. Association of RBM7 with RNAPII-derived RNAs enables degradation upon emergence of unprotected RNA 3′ ends. Thus, the NEXT complex defines an early exosome targeting pathway acting on newly synthesized RNA, including snoRNAs embedded in pre-mRNA introns.

Highlights

- RBM7 is loaded promiscuously onto newly synthesized RNA
- RBM7/NEXT defines an early nuclear RNA decay pathway
- RBM7/NEXT triggers exosome activity at snoRNA-encoding introns
- RBM7/NEXT assigns many lncRNAs for nuclear degradation

Accession Numbers

GSE63791
GSE63496
GSE52132
GSE48286

Lubas et al., 2015, Cell Reports *10*, 178–192
January 13, 2015 ©2015 The Authors
http://dx.doi.org/10.1016/j.celrep.2014.12.026

OPEN ACCESS
CellPress

Cell Reports
Article

The Human Nuclear Exosome Targeting Complex Is Loaded onto Newly Synthesized RNA to Direct Early Ribonucleolysis

Michal Lubas,[1,2,3,5,6] Peter Refsing Andersen,[1,5,7] Aleks Schein,[1,8] Andrzej Dziembowski,[2,3] Grzegorz Kudla,[4] and Torben Heick Jensen[1,*]

[1]Centre for mRNP Biogenesis and Metabolism, Department of Molecular Biology and Genetics, Aarhus University, 8000 Aarhus, Denmark
[2]Institute of Biochemistry and Biophysics, Polish Academy of Sciences, 02-106 Warsaw, Poland
[3]Department of Genetics and Biotechnology, Faculty of Biology, University of Warsaw, 02-106 Warsaw, Poland
[4]MRC Human Genetics Unit, Institute of Genetics and Molecular Medicine, University of Edinburgh, Edinburgh EH4 2XU, UK
[5]Co-first author
[6]Present address: Biotech Research and Innovation Centre, University of Copenhagen, 2200 Copenhagen, Denmark
[7]Present address: Institute of Molecular Biotechnology of the Austrian Academy of Sciences, 1030 Vienna, Austria
[8]Present address: Division of Genomic Technologies, RIKEN, Yokohama 230-0045, Japan
*Correspondence: thj@mb.au.dk
http://dx.doi.org/10.1016/j.celrep.2014.12.026

SUMMARY

The RNA exosome complex constitutes the major nuclear eukaryotic 3′-5′ exonuclease. Outside of nucleoli, the human nucleoplasmic exosome is directed to some of its substrates by the nuclear exosome targeting (NEXT) complex. How NEXT targets RNA has remained elusive. Using an in vivo crosslinking approach, we report global RNA binding sites of RBM7, a key component of NEXT. RBM7 associates broadly with RNA polymerase II-derived RNA, including pre-mRNA and short-lived exosome substrates such as promoter upstream transcripts (PROMPTs), enhancer RNAs (eRNAs), and 3′-extended products from snRNA and replication-dependent histone genes. Within pre-mRNA, RBM7 accumulates at the 3′ ends of introns, and pulse-labeling experiments demonstrate that RBM7/NEXT defines an early exosome-targeting pathway for 3′-extended snoRNAs derived from such introns. We propose that RBM7 is generally loaded onto newly synthesized RNA to accommodate exosome action in case of available unprotected RNA 3′ ends.

INTRODUCTION

Nuclear RNA metabolism in eukaryotes depends to a large extent on the 3′-5′ exoribonucleolytic and endoribonucleolytic activities of the RNA exosome complex (Chlebowski et al., 2013; Schneider and Tollervey, 2013). In vivo exosome activity is regulated by associated enzymatic cofactors and RNA-binding adapters, which facilitate exosome access and recruitment to a multitude of substrates. The best characterized cofactor of the nuclear exosome is the *S. cerevisiae* Trf4p/5p-Air1p/2p-Mtr4p polyadenylation (TRAMP) complex, containing either one of two oligo(A)-polymerases Trf4p/Trf5p and zinc finger proteins Air1p/Air2p, respectively, as well as the DEAD box RNA helicase Mtr4p (LaCava et al., 2005; Vanácová et al., 2005; Wyers et al., 2005). TRAMP is recruited to substrates by the exosome adaptor- and RNA-binding Nrd1p/Nab3p/Sen1p (NNS) protein complex (Arigo et al., 2006; Thiebaut et al., 2006; Vasiljeva and Buratowski, 2006). While TRAMP predominantly acts to promote exosomal decay by the oligoadenylation and unwinding of RNA targets, the RNA polymerase II (RNAPII)-binding NNS complex targets short sequence motifs in the nascent RNA to trigger RNAPII transcription termination and to couple this process with the handover of substrates with free 3′ ends to TRAMP (Arigo et al., 2006; Carroll et al., 2007; Steinmetz et al., 2001; Thiebaut et al., 2006; Tudek et al., 2014).

Although the principal inner workings of the nuclear exosome machinery appear similar in mammalian cells with the Mtr4p homolog, hMTR4/SKIV2L2, as a central helicase coupling the activity of the exosome to its RNA adapters, the spatial organization and nature of exosome accessory factors have diverged considerably from *S. cerevisiae* (Lubas et al., 2011; Sloan et al., 2012; Wolin et al., 2012). In mammals, two distinct exosome cofactors have so far been characterized, which are the nucleolar-localized hTRAMP complex (Fasken et al., 2011; Lubas et al., 2011) and the nucleoplasm-specific Nuclear EXosome Targeting (NEXT) complex (Lubas et al., 2011). Sharing hMTR4 with hTRAMP, the otherwise distinct trimeric NEXT complex is further composed of the RNA recognition motif (RRM)-containing RBM7 and the zinc-knuckle ZCCHC8 proteins. Consistent with their different nuclear localization, hTRAMP and NEXT complexes operate on different RNA substrates. While hTRAMP is involved in oligoadenylation of nucleolar rRNAs to facilitate their decay, depletion of NEXT subunits leads to the stabilization of nuclear exosome substrates such as PROMoter uPstream Transcripts (PROMPTs) and 3′-extended products from U1/U2 snRNA- and replication-dependent histone (RDH) genes (Andersen et al., 2013; Lubas et al., 2011; Ntini et al., 2013; Shcherbik et al., 2010). How

the NEXT complex reaches its nucleoplasmic RNA targets is a central question as no NNS-homologous complex has been identified in metazoan systems.

A possible clue to NEXT-substrate targeting came recently when a robust interaction between NEXT and the RNA cap-binding complex (CBC) was revealed (Andersen et al., 2013; Hallais et al., 2013). Specifically, all NEXT components individually copurify the CBC as well as the CBC-associated arsenic-resistance 2 (ARS2) and ZC3H18/NHN1 proteins, forming the so-coined CBC-NEXT (CBCN) protein assembly. This link between the CBC and NEXT provides a direct coupling between the capped 5′ ends of RNAPII transcripts and 3′ end processing/degradation processes. A similar connection was reported between the *S. cerevisiae* NNS and CBC complexes (Vasiljeva and Buratowski, 2006); however, the extent to which this interaction guides the NNS complex to RNAPII transcription units has not been further explored. Interestingly, a subcomplex of the CBCN assembly, the CBC-ARS2 (CBCA) complex, triggers the termination of PROMPT, U2, and RDH gene read-through transcription, whereas depletion of NEXT components RBM7 and ZCCHC8 shows only modest transcription phenotypes (Andersen et al., 2013; Hallais et al., 2013). While this provides some mechanistic analogy to the *S. cerevisiae* system with its coupling of transcription termination and exosomal decay, it still leaves open the mechanism by which NEXT seeks out its targets, including how it organizes RNA binding with summoning of the exosome.

Here, we used an individual-nucleotide-resolution UV crosslinking and immunoprecipitation (iCLIP) procedure to achieve a transcriptome-wide view of in vivo RBM7-RNA interactions. Our results demonstrate that RBM7 associates broadly with RNAPII-derived RNA, thereby enabling transcript degradation upon emergence of unprotected RNA 3′ ends. We suggest that the NEXT complex defines an early exosome targeting pathway acting on newly synthesized RNA.

RESULTS

Global Overview of RBM7-RNA Interactions

To achieve a transcriptome-wide view of in vivo NEXT interactions, we performed iCLIP (Figure 1A) (Konig et al., 2011) to map RNA-binding sites of the RRM-containing (Figure S1A) and vertebrate-conserved (Figure S1B) RBM7 protein. Localization and affinity purification (LAP)-tagged RBM7 expressed at near-endogenous levels in HeLa cells (Andersen et al., 2013) crosslinked to RNA with an efficiency comparable to the RNA-binding protein hnRNPK (Figure S1C, lanes 2 and 3). Extensive treatment with either RNase I or RNase TI confirmed that the majority of the ^{32}P-labeled RNA was attached to RBM7-LAP (Figure S1D), although its stable interaction partner, ZCCHC8, was also present in the IP eluates (Figure S1E, lanes 5–8). Notably, hMTR4 was absent after the stringent washing conditions employed, indicating a strong interaction between ZCCHC8 and RBM7. As expected, RBM7 only crosslinked to RNA in the presence of UV irradiation (Figure S1F). RBM7 iCLIP was carried out in two replicates, which were either treated with control luciferase siRNAs or siRNAs targeting the exosome core-component hRRP40 (Figure S1G) to enable visualization of exosome substrates and RBM7-binding targets in the same experimental setup. The nontagged control cell line did not generate detectable PCR products (Figure 1A), implying a low experimental background. For further comparative analysis, we included our previously published RNA sequencing (RNA-seq) datasets of total rRNA-depleted RNA obtained from HeLa cells treated with siRNAs targeting hRRP40, ZCCHC8, or EGFP (control) (Andersen et al., 2013).

To provide a first overview of the data, unique RBM7 iCLIP and corresponding RNA-seq reads from control and hRRP40-depleted samples were distributed into general genomic categories: pre-mRNA intron, long noncoding RNA (lncRNA), repetitive elements, pre-mRNA exon, short ncRNA (miRNA, snoRNA, tRNA, snRNA), unannotated rRNA, and "other" (Figure 1B). Within pre-mRNA, the majority of RBM7 iCLIP tags mapped to introns (37%–43%) and a smaller fraction to exons (8%–11%). The RNA-seq data showed a ~3-fold higher frequency of reads in exons (30%). Such relative enrichment of intronic reads in RBM7 iCLIP over RNA-seq data are in line with the nucleoplasmic localization of RBM7 (Lubas et al., 2011). Similar intron/exon distributions of iCLIP-tags were observed in studies of splicing-related (FUS, U2AF65, and SFSF3/4) (Änkö et al., 2012; Rogelj et al., 2012; Zarnack et al., 2013), but not cytoplasmic (UPF1), RNA-binding proteins (Zünd et al., 2013). This indication of RBM7 binding, before or during pre-mRNA splicing, was supported by inspection of representative protein-coding genes (see Figure 1C, "red tracks" for the *CKS2* and *SECISBP2* genes, and further examples below).

Another large fraction of iCLIP tags mapped to a broadly defined collection of lncRNAs (GENCODE v18) (Figure 1B). Unique tag numbers increased upon exosome depletion from 14% (RBM7) to 20% (RBM7/hRRP40), likely reflecting a prolonged association between lncRNA transcripts and the NEXT complex in the absence of exosome-mediated lncRNA decay (Andersson et al., 2014b; Lubas et al., 2011). Consistent with this notion, the *CKS2* and *SECISBP2* loci also revealed evidence for a physical contact between RBM7 and the transcription start site (TSS)-proximal PROMPTs of these genes (Figure 1C, "blue" tracks), further validated by RNA IP (RIP) of two previously reported PROMPTs (Figure S1H).

Of the remaining genomic categories, "repetitive elements" constituted a noteworthy class of RBM7-bound transcripts of which comprehensive analyses fall beyond the scope of this study. Additionally, notable crosslinking of RBM7 to stable ncRNAs (tRNA, rRNA, snoRNA, and snRNA) was observed. Mature forms of these transcripts are highly abundant and offer binding sites for RNA binding proteins calling the specificity of the interaction into question. Binding to the unprocessed forms of short ncRNAs, specifically snRNA and snoRNA, is addressed in detail later (see below).

Finally, RBM7 iCLIP tags were found to harbor notably fewer nonencoded 3′-terminal adenines than that from CLIP tags of yeast exosome cofactors (~1% versus 6%–30%) (Tuck and Tollervey, 2013; Wlotzka et al., 2011). This likely reflects a requirement in *S. cerevisiae* for the posttranscriptional addition of 3′ adenines to promote exosomal activity. In human cells, such a requirement mostly appears to be relevant in nucleoli (Lubas et al., 2011; Preker et al., 2011). Therefore, increased

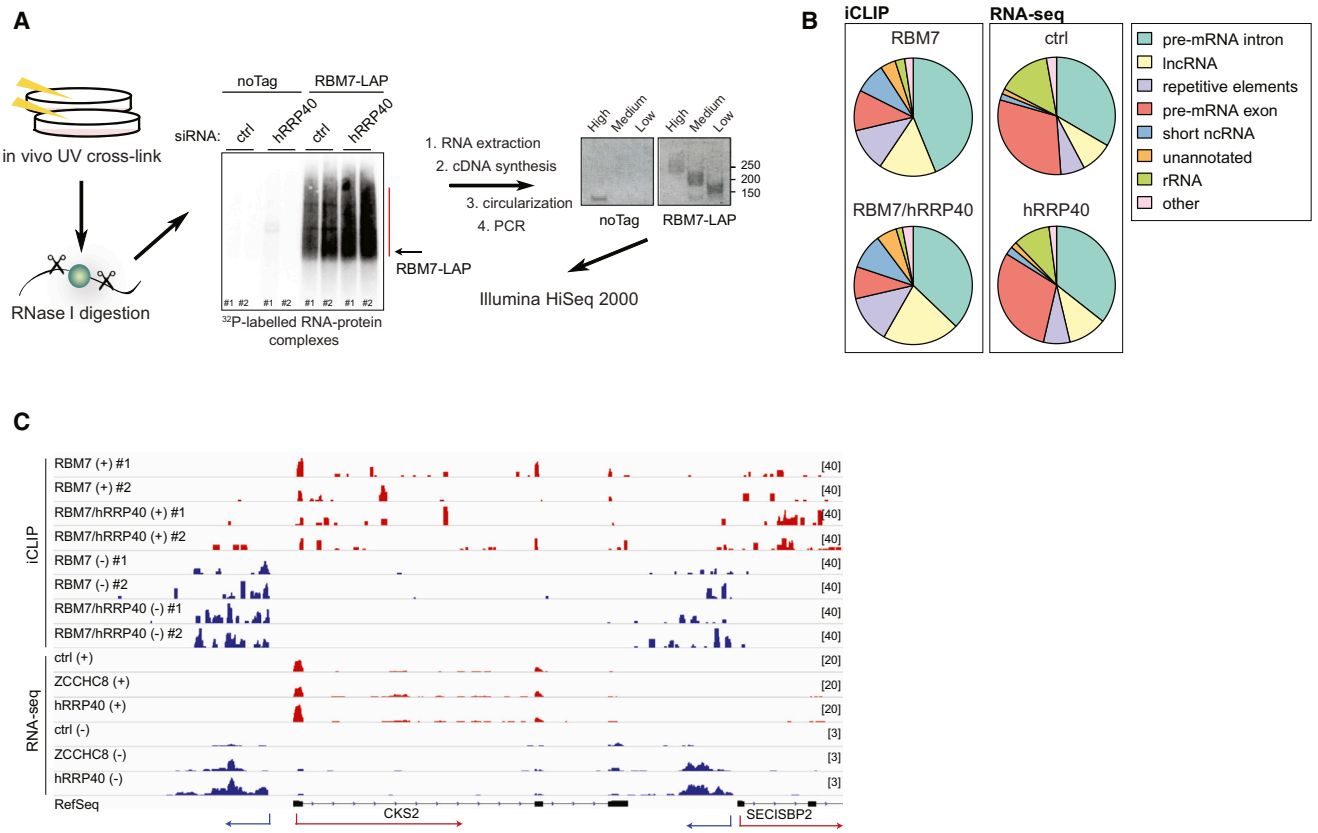

Figure 1. iCLIP Reveals Direct In Vivo Targets of RBM7

(A) Schematic overview of the iCLIP procedure. Control ("noTAG") and RBM7-LAP HeLa cells were transfected with luciferase (control [ctrl]) or hRRP40 siRNA and UV irradiated at 254 nm. Crosslinked RNA-protein complexes were purified, subjected to RNase I treatment, and analyzed by SDS-PAGE. Visualized by P^{32} autoradiography, RBM7-linked RNAs are indicated by a red line, and the black arrow denotes the RBM7-LAP molecular weight; #1 and #2 indicate the two biological replicates. Extracted RNA material was used for preparation of three size fractions of RT-PCR products (high, medium, low) and pooled prior to sequencing.

(B) Distribution charts of unique tags derived from the iCLIP (RBM7 and RBM7/hRRP40) and RNA-seq (ctrl and hRRP40) libraries and mapped to the indicated RNA classes (averages from the two biological repeats).

(C) Genome browser screenshot of RBM7 iCLIP and RNA-seq reads mapped to a representative genomic area encompassing TSS-proximal regions of two protein-coding genes (CKS2 and SECISBP2). Four RBM7 iCLIP (eight tracks) and three RNA-seq (six tracks) libraries are visualized by (−) (blue) and (+) (red) strands. Numbers to the right show the normalized maximum read count value.

3′ adenylation of RBM7 iCLIP tags from lncRNA, snRNA, and mRNA intron fractions upon hRRP40 depletion (Figure S1I) probably arises from adenylation of nuclear targets incapable of turning over efficiently in the absence of exosome activity.

Taken together, these initial analyses confirmed that RBM7 physically contacts known nuclear RNA exosome substrates, validating the utilized RBM7 iCLIP procedure to reliably describe the detailed in vivo RNA interaction profile of RBM7.

RBM7 Poises lncRNAs for Exosomal Decay via Initial CBC Contacts

That RBM7/NEXT recruits the exosome to nuclear substrates has previously been suggested by the direct physical interaction of RBM7/NEXT with the exosome (Lubas et al., 2011), the upregulation of similar substrate classes upon exosome and NEXT depletion (Andersen et al., 2013; Lubas et al., 2011), and the interaction of CBCN with exosome substrates (Andersen et al., 2013). To obtain experimental support that transcripts physically interacting with RBM7 are ultimately degraded by the exosome, we analyzed iCLIP and RNA-seq data for (1) a set of 12153 PROMPT regions, (2) their neighboring genic regions, and (3) 10,014 HeLa cell enhancer RNAs (eRNAs) detectable within both the iCLIP and RNA-seq data as well as in data sets of RNA 5′ ends generated by Cap Analysis of Gene Expression (CAGE) (Andersson et al., 2014b; Ntini et al., 2013). Like PROMPTs, eRNAs are capped, short, usually unspliced, and exosome sensitive (Andersson et al., 2014a, 2014b; De Santa et al., 2010; Kim et al., 2010). To address RBM7-binding, we normalized control HeLa RBM7 iCLIP- to RNA-seq-read coverage within 1 kb from the TSSs of the interrogated RNAs. This revealed a higher density of RBM7 on PROMPTs and eRNAs relative to genic transcripts (Figure 2A, left). Less relative binding of RBM7 to genic RNA is likely due to high levels of unbound cytoplasmic mRNA as our iCLIP data later revealed that RBM7 preferentially binds pre-mRNA (Figures 3A and 5B). As expected, PROMPTs and eRNAs were also generally

stabilized upon hRRP40 (Figure 2A, middle) and ZCCHC8 (Figure 2A, right) depletions. This implies that RBM7 targeting of these transcripts results in their subsequent degradation by the RNA exosome. We next asked whether this correlation between RBM7 binding and exosome sensitivity could also be observed at the level of individual transcripts. To this end, we plotted RBM7 iCLIP enrichment of each transcript (the ratio of RBM7 iCLIP to control RNA-seq signal) against its sensitivity to exosome (hRRP40) or NEXT (ZCCHC8) depletion (the ratio of hRRP40 or ZCCHC8 RNA-seq to control RNA-seq signals) (Figure 2B). This showed that also for individual transcripts, levels of RBM7 binding correlate with sensitivity to hRRP40 and ZCCHC8. Individual examples of PROMPTs (Figure S2A) and eRNAs (Figure S2B) were inspected and confirmed this conclusion.

To attract the exosome to its substrates, NEXT needs first to bind RNA. Our discovery of a CBCN interaction led to the hypothesis that the CBC may constitute one mechanism to recruit NEXT to capped transcripts. To test this idea, we performed RBM7-RIP of four known exosome substrates (three PROMPTs and 3′-extended U1 snRNA) as well as two transcripts not known to be exosome targets (GAPDH mRNA and pre-mRNA) in control cells or in cells depleted of both CBC subunits (CBP80 and CBP20) (Figure S2C). While comparable amounts of RNA were purified with RBM7 from untreated and CBC-depleted cells (data not shown) and while the largely cytoplasmic GAPDH mRNA was unchanged between the two conditions, depletion of the CBC resulted in an ~50% decrease in RBM7-associated GAPDH pre-mRNA and 3′-extended U1 snRNA (Figure 2C). Strikingly, for the tested PROMPTs, CBC depletion resulted in a pronounced decrease in RBM7-bound material (Figure 2C), which was especially prominent taking into account that these transcripts increase in abundance upon CBC depletion (Figure S2D). Taken together, these data suggest that the CBC aids in recruiting the NEXT complex newly synthesized RNAPII transcripts.

RBM7 recruitment to RNA could also be favored by transcript sequence. To analyze this possibility, we determined enriched pentamer sequences of all RBM7 iCLIP crosslinking sites as well as those specifically mapping to PROMPTs or introns. For all RNA sets, some preference for U-rich sequences could be detected (Figure 2D, top panel). Although these can result from a UV crosslinking bias (Sugimoto et al., 2012), their abundance was higher than in previously published DGCR8 and U2AF65 iCLIP datasets, which we reanalyzed (Figure 2D, bottom panels). Instead of, or in addition to, using the CBC for transcript targeting, RBM7 may also take advantage of U-rich sequences.

TSS-Proximal Regions Are Broadly Targeted by RBM7

We next profiled RBM7-binding over regions expressing different RNA species. First, we calculated RBM7 iCLIP read coverage values over the above-mentioned genic promoter regions. Profiling RBM7 binding in a 3 kb window on either side of these TSSs revealed an enrichment for TSS-proximal positioning in both sense and antisense directions (Figure 3A, left). A more modest accumulation of RBM7 was seen around poly(A) sites (also known as "3′ ends of the annotated genes" [EAGs]) (Figure 3A, right). A similar profile emerged when plotting the direct RBM7-RNA crosslinking sites as defined by reverse transcriptase road blocks in the sequence reads (Figure S3A). Consistent with the RNA-seq data (Figure 3B), iCLIP data exhibited an increased coverage of PROMPT regions upon depletion of hRRP40 (compare Figures 3A and 3B, left). Exosome sensitivity was less pronounced in the sense direction from TSSs, likely due to the lower frequency of premature termination events taking place compared with the antisense direction (Ntini et al., 2013). Still, when removing exonic reads to enrich for nuclear transcripts, a "PROMPT-like" stabilization phenotype was observed upon hRRP40 or ZCCHC8 depletion (Figure 3B, right). To address whether such prematurely terminated RNAs would bind RBM7, we sorted RNA-seq signal detected within 1 kb downstream of sense TSSs by its ZCCHC8 sensitivity ("unchanged" or "upregulated"), which revealed that ZCCHC8 sensitivity generally correlated with higher RBM7 occupancy as determined by iCLIP (Figure S3B, left). Moreover, employing published 3′-end sequencing data (3′ TAG-seq) (Ntini et al., 2013), we observed a correlation between the frequency of early 3′ ends and an increased density of RBM7 iCLIP tags in these regions (Figure S3B, right). Thus, despite early 3′-end formation often being suppressed in the sense direction of transcription (Ntini et al., 2013), we suggest that the NEXT complex also here surveys early transcription termination events to target abortive transcripts for exosomal degradation.

We next analyzed RBM7 association with eRNAs, which are most often bidirectionally transcribed from common transcription initiation regions and sensitive to exosome-activity in both directions (Andersson et al., 2014b). Consistent with a role of the NEXT complex in the degradation of eRNAs, ZCCHC8 depletion increased their levels (Figure 3C, top image), and RBM7 iCLIP signal in these regions was prominent in control cells and increased in the absence of hRRP40 (Figure 3C, bottom image; compare with Figure S3C). As in the case of PROMPTs, RBM7 iCLIP tags displayed a narrow distribution around eRNA TSSs consistent with the general similarity between the biogenesis and turnover of these lncRNAs (Andersson et al., 2014b; Ntini et al., 2013).

PROMPTs and eRNAs are most often intron-less. To expand our analysis to intron-containing lncRNAs, we investigated RBM7 occupancy over a set of annotated lncRNAs (GENCODE v18) that are expressed in HeLa cells (Andersson et al., 2014a) and divided these into monoexonic and polyexonic transcripts. For both transcript classes, RBM7 signal in PROMPT regions increased upon hRRP40 depletion (Figure 3D). Interestingly, only intron-less lncRNAs displayed a similarly strong hRRP40-sensitivity (Figure 3D, (+) directions of top and bottom images), whereas intron-containing lncRNAs showed a RBM7 iCLIP profile like for all genic transcripts (Figure 3A). Consistent with previous observations (Ntini et al., 2013), this suggests that the presence of introns generally renders RNAs less exosome sensitive.

In summary, RBM7 avidly targets RNAPII-derived transcripts of even short length with enrichment toward RNA 5′ ends, supporting the notion that CBC-aided NEXT recruitment may be universal. While recruitment of the NEXT complex to the investigated lncRNAs most often will lead to exosome-mediated decay, we stress that RBM7 binding per se does not trigger

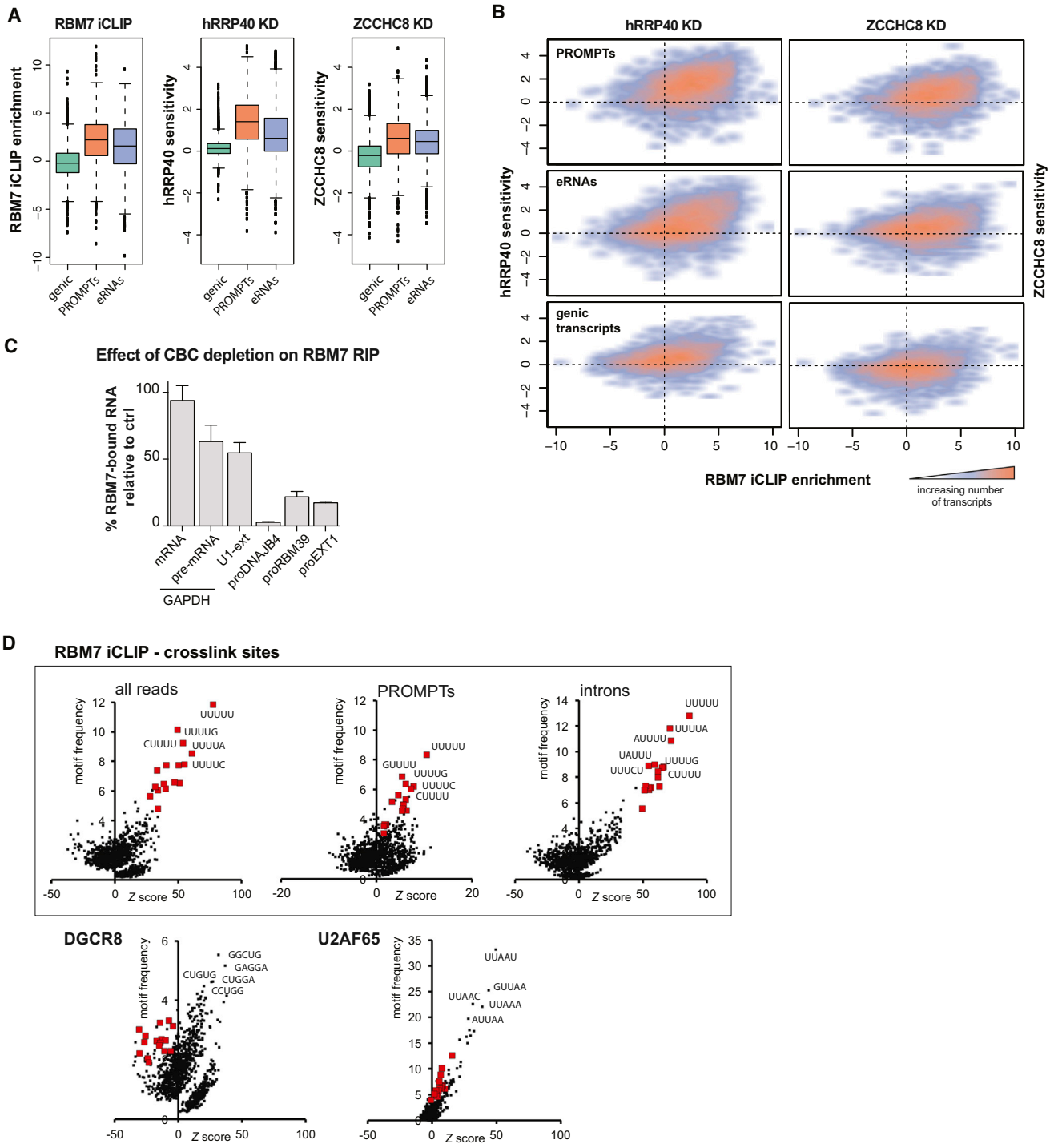

Figure 2. Factors Determining RBM7 Recruitment to RNA

(A) Box plots showing RBM7 iCLIP enrichment (log2(RBM7[iCLIP]) RPM/control[RNA-seq] RPM)) (left), hRRP40 (middle), and ZCCHC8 (right) sensitivity (log2(siRNA knockdown(RNA-seq) RPM/control(RNA-seq) RPM) of the first 1 kb of 12,153 genic RNAs, their associated PROMPTs, and 10,014 eRNA regions as indicated. RPM, reads per million; KD, knockdown. Note a slight overall decrease in genic transcripts upon ZCCHC8 depletion, the nature of which is unknown.

(B) Heat graphs showing RBM7 iCLIP enrichment versus hRRP40 (left) or ZCCHC8 (right) sensitivities calculated as in (A) and for individual transcripts contained in the (A) box plots.

(C) Quantitative RT-PCR analysis of RBM7-RIP'ed RNA purified from CBP80/CBP20-depleted or untreated HeLa cells. PROMPTs (*proDNAJB4*, *proRBM39*, and *proEXT1*), the unstable 3′-extended U1snRNA (U1-ext), *GAPDH* pre-mRNA, and the mainly cytoplasmic *GAPDH* mRNA were analyzed as indicated. The graph

(legend continued on next page)

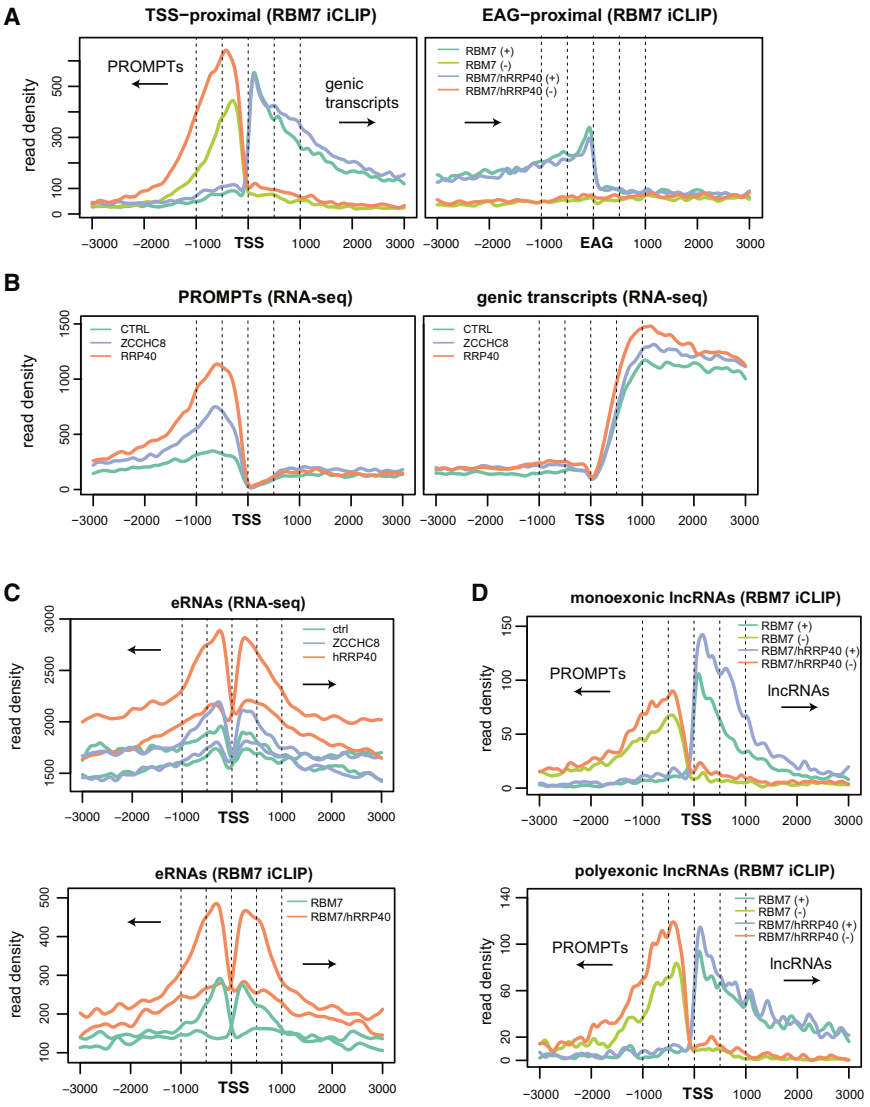

Figure 3. RBM7 Binds TSS-Proximal Transcripts

(A) Density profiles of RBM7 iCLIP reads over regions of 3 kb upstream and downstream of TSSs (left) and EAGs (right) from 12,153 genes. Transcription directions are indicated by arrows. Different samples and their (+) versus (−) strand orientations are indicated.

(B) Density profiles of RNA-seq reads from genomic regions used in (A). To reduce signal from the abundant pool of cytoplasmic RNA, reads mapping to exon annotations from RefSeq and ENSEMBL were filtered before density calculation. Left and right images show (−) and (+) strand reads, respectively.

(C) Density profiles of RNA-seq (top) and RBM7 iCLIP (bottom) reads in a region of 3 kb upstream and downstream of initiation regions of 10,014 eRNAs expressed in the displayed datasets. Data are plotted as in (A).

(D) Density profiles of RBM7 iCLIP reads over regions of 3 kb upstream and downstream of TSSs of monoexonic (left) or polyexonic (right) lncRNAs plotted as in (A).

transcript turnover, as exemplified by the robust binding of RBM7 to intron-containing RNA.

RBM7 Targets 3′-Extended Products from Intron-less RNAPII Genes

Having observed RBM7 binding to lncRNAs, we asked whether other short RNAPII-derived RNAs would be equally targeted. For this purpose, UsnRNA- and RDH genes were chosen as these produce intron-less RNAPII transcripts of <1,000 nt. Stable 3′-end formation of these transcripts proceeds through cleavage by the endonucleases CPSF73 (RDHs) and CPSF73L (most U snRNAs), residing in processing complexes, which deal with short transcription units. This is a noteworthy distinction to PROMPTs and eRNAs that appear to utilize at least parts of the mRNA 3′-end processing apparatus placed out of context, a feature that has been suggested to contribute to the unstable nature of these RNAs (Andersen et al., 2013; Andersson et al., 2014b; Hallais et al., 2013; Ntini et al., 2013).

We used RBM7-RIP to assess RBM7-binding to U5 snRNA, which among other snRNAs was enriched in the RBM7 iCLIP data upon exosome inhibition (Figure 4A). The RBM7-RIP assay reliably detected RBM7 targets (Figure 2C), which could also be revealed by northern blotting analysis of the NEXT/exosome-sensitive PROMPT proDNAJB4 (Figure S4A, left), the heterogeneous species of which were precipitated (Figure S4A, right). Such RBM7 binding and NEXT/exosome sensitivity was confirmed by the respective sequence data sets (Figure S4B). Changing to a northern probe targeting U5 snRNA, some specific RBM7 binding to mature U5 could be seen, which was not markedly affected by exosome depletion (Figure 4B, left, lanes 3–6). However, exosome-sensitive RBM7 interaction with longer U5 species was clearly visible (Figure 4B, left, compare lanes 5 and 6) and even more apparent when employing a probe detecting hRRP40-sensitive 3′-extended U5 snRNAs (Figure 4B, right).

displays the fraction of RBM7-bound RNA following depletion of CBP80/CBP20, normalized to input and RNA levels in control. Mean values were quantified from triplicate RT-PCR experiments of two biological replicates with bars representing SEM.

(D) Enrichment scores (x axes) and frequencies (y axes) of 5-mer motifs in 21 nt regions centered at RBM7 crosslinking sites calculated for all mapped reads (top left), reads overlapping PROMPTs (top middle), or introns (top right). Motif analyses of DGCR8 and U2AF65 are included for comparison (bottom). Motifs containing four or more uridines are marked in red; all other pentamers are black.

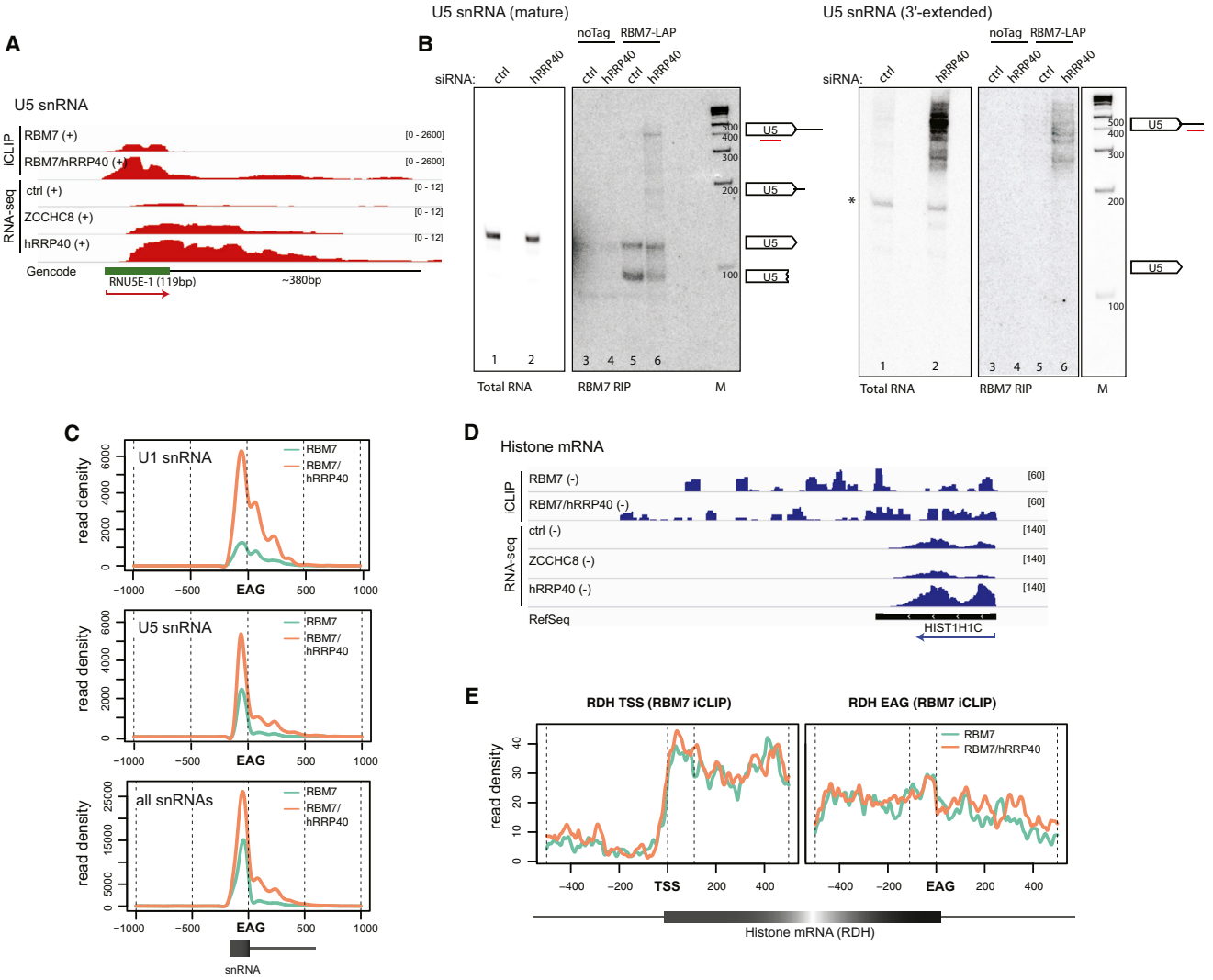

Figure 4. RBM7 Targeting of 3′-Extended RNAs

(A) Genome browser screenshot of RBM7 iCLIP and RNA-seq reads mapped to a representative U5 snRNA region (RNU5E-1 gene). The labeling is as shown in Figure 1C. Only the (+) strand is shown.

(B) U5 snRNA Northern blotting analysis of total RNA of hRRP40 or luciferase (control) siRNA treated cells (left) or RBM7-RIP'ed RNA from similar samples (right). Northern membranes were incubated with a probe targeting the mature (left) or 3′-extended (right) parts of U5 snRNA, as indicated by red lines on arrowed boxes symbolizing relevant U5 species.

(C) Density profiles of RBM7 and RBM7/hRRP40 iCLIP reads over U1 and U5 snRNA genes as well as combined snRNA gene annotations ("snRNA all").

(D) Genome browser screenshot of RBM7 iCLIP and RNA-seq reads mapped to the HIST1H1C RDH RNA. The labeling is as shown in Figure 1C; only the (−) strand is shown.

(E) Density profiles of RBM7 and RBM7/hRRP40 iCLIP reads over a region spanning 0.5 kb upstream and downstream of the TSSs (left) and EAGs (right) of RDH loci.

RBM7 also interacted with a species of shorter length than mature U5 snRNA of unclear nature (Figure 4B, left, lanes 3–6). We conclude that RBM7 binds to mature U5 snRNA and to its 3′-extended products that are likely unprocessed precursors of U5 or transcriptional read-through products (Cuello et al., 1999). As for PROMPTs and eRNAs, RBM7 binding to the 3′-extended species suggested its participation in eliciting their efficient trimming/removal by the exosome. This observation was corroborated by similar interactions of RBM7 with exosome-sensitive 3′-extended species of U1 snRNA from the RNU1-59P gene (Figures S4C and S4D) and of U4ATAC snRNA (Figures S4E and S4F). Moreover, it was supported at a global level by mapping of RBM7 iCLIP reads to all U1 and U5 snRNA genes (Figure 4C, top and middle), as well as to all snRNA genes (Figure 4C, bottom).

We then turned to RDH genes. As for tested U snRNA genes, RNAPII transcription at these loci can proceed up to 1 kb past their EAGs (Anamika et al., 2012). Furthermore, the absence of

an intact CBCA complex increases the abundance of RDH mRNAs extending beyond their EAGs, which leads to their efficient targeting by the RNA exosome (Andersen et al., 2013; Gruber et al., 2009). Indeed, RBM7 was amply distributed along the 3′ extensions of three selected RDH transcripts (Figures 4D, S4G, and S4H), an observation that was generalized by RDH metagene analysis (Figure 4E). The RBM7-bound and 3′-extended RDH mRNAs were not evidently targeted by the RNA exosome (Figures 4D and 4E). A similar conclusion could be drawn from the RNA-seq data, which otherwise confirmed a previous notion of exosome-dependent turnover of mature RDH mRNA (Figures 4D, S4G, and S4H; Reis and Campbell, 2007). We suggest that loading of RBM7/NEXT onto RDH transcripts enables rapid targeting by the nuclear exosome, which only occurs upon lowered 3′-end processing efficiency. Separate analysis of mature and 3′-extended RDH RNA levels confirmed that decay of mature histone RNA is largely NEXT-independent (Figure S4I) and likely relies on the cytoplasmic RNA exosome (Reis and Campbell, 2007). A minor increase of, presumably nuclear, 3′-extended histone RNA could be detected upon ZCCHC8 depletion. We suggest this pool arises due to unsuccessful 3′-end processing of these RNAs.

Taken together, the data add 3′-extended Usn- and RDH-mRNAs to the range of targets bound by RBM7 early in their life cycle.

RBM7 Targets Pre-mRNA and Accumulates at Intron 3′ Ends

So far we reported RBM7 interactions with RNAs for which most are ultimately targeted by the RNA exosome. As shown in Figures 2A, 2B, and 3A, this is not always the case, and we therefore analyzed RBM7 distribution on protein coding transcripts in more detail. Given that RBM7 iCLIP tags mapped to both introns and exons (Figures 1B and 1C), we first plotted the data against 10,811 pre-mRNAs sorted by increasing first exon length. While this analysis confirmed the previously noticed bias of RBM7 binding toward RNA 5′ ends, it did not reveal a noticeable distinction between targeting of first exons and subsequent introns (Figure 5A), suggesting that RBM7 establishes RNA contacts prior to splicing. To confirm this possibility, we counted iCLIP tags overlapping unspliced (intron-exon [IE] and exon-intron [EI] borders) and spliced (exon-exon [EE] borders) RNA and also included the RNA-seq data for comparison. The calculated high ratios of IE and EI to EE spanning reads in the iCLIP libraries as compared with the RNA-seq libraries strongly indicate that RBM7-bound RNA is generally unspliced (Figure 5B, left). This was supported by a low fraction of EE spanning iCLIP reads, demonstrating that RBM7 is generally depleted from spliced mRNA (Figure 5B, right). Similarly high unspliced/spliced RNA ratios were reported for the yeast RNA surveillance factors Mtr4p and Trf4p as well as for the CBC (Schneider et al., 2012; Tuck and Tollervey, 2013), which associates early with pre-mRNA. Bearing the avid interaction of RBM7 with PROMPTs and eRNAs in mind, these data considerably strengthen the hypothesis that RBM7 targets newly synthesized RNA.

To gain insight into which tasks RBM7 may exercise when bound to pre-mRNA, we investigated where in intronic regions RBM7 iCLIP tags are positioned. The distribution of iCLIP read densities was plotted in regions of 500 bp upstream and downstream of exon-intron borders, removing first and last introns to prevent possible biases due to RBM7 interaction with RNA termini (Figure 3A). Interestingly, RBM7 binding was generally enriched at the 3′ ends of introns, independent of exon and/or intron length (Figure 5C, right). Accumulation of iCLIP tags in the 3′ ends of upstream exons was also observed, but only for short exons (Figure 5B, left), suggesting that this signal originates from RBM7 accumulation at 3′ ends of preceding introns. Notably, most RBM7 iCLIP reads mapping around 3′ splice sites (SSs) traversed IE borders (data not shown), meaning that they primarily derive from pre-mRNAs as opposed to excised introns. We speculate that this intronic 3′-end enrichment of RBM7 may, at least partly, be explained by a RBM7 preference for uridines (Figure 2D).

To investigate what role RBM7 may be playing at introns, we first focused on introns from which miRNAs are cotranscriptionally processed (Morlando et al., 2008). Interrogating RBM7 binding to intronic pre-miRNAs, we noted an enrichment of RBM7 iCLIP tags at pri-miRNA 5′ flanks (Figure 5D). Analysis of a curated pre-miRNA dataset (miRBase) confirmed this finding (Figure 5E). We therefore suggest that the NEXT complex partakes in 3′-5′ exosomal decay of the intronic pre-miRNA 5′ flanks. Thus, although using the NEXT/exosome axis for some purpose of RNA decay, miRNA-containing introns are not likely drivers of the enriched RBM7 signal at intronic 3′ ends.

NEXT Is Targeted to snoRNA-Encoding Introns

Other prominent human intron-contained ncRNAs are the snoRNAs, the vast majority of which are encoded within introns. Previous efforts revealed that splicing is required for human snoRNA biogenesis (Hirose et al., 2003) and suggested a role for 5′-3′ and 3′-5′ exonucleolysis in their processing (Berndt et al., 2012; Kiss and Filipowicz, 1995). Therefore, we plotted the distribution of RBM7 iCLIP reads over intronic regions flanking snoRNAs and found an increased signal at these 3′ ends, which was enriched upon hRRP40 depletion (Figure 6A). In support of a role of the NEXT/exosome complexes on these introns subsequent to pre-mRNA splicing, hRRP40 depletion led to an increased number of genuine intronic reads as compared with those spanning IE borders (Figure S5A). Inspection of individual snoRNA host genes supported this observation (Figures 6B and S5B–S5D) and further revealed that RBM7 binding, in the absence of the exosome, was enriched toward the very 3′ ends of introns likely representing the 3′ ends of snoRNA precursors.

RNA-seq data provided further support that the observed RBM7 binding can elicit exosomal decay/processing, in that accumulation of reads spanning the 3′-extended snoRNAs increased upon both ZCCHC8 and hRRP40 depletion (Figure 6B). This implies that NEXT/exosome controls the metabolism of intronic snoRNA through binding of RBM7 to emerging 3′ ends. Given the otherwise uniform distribution of RBM7 along pre-mRNA, this suggests a delay between early binding of RBM7 and 3′-5′ intron decay by the RNA exosome. We do not observe a general increase of intronic RBM7 signal or intron RNA accumulation upon hRRP40 depletion, which is most likely due to rapid 5′-3′ decay/processing of introns by the exoribonuclease XRN2 (Valen et al., 2011).

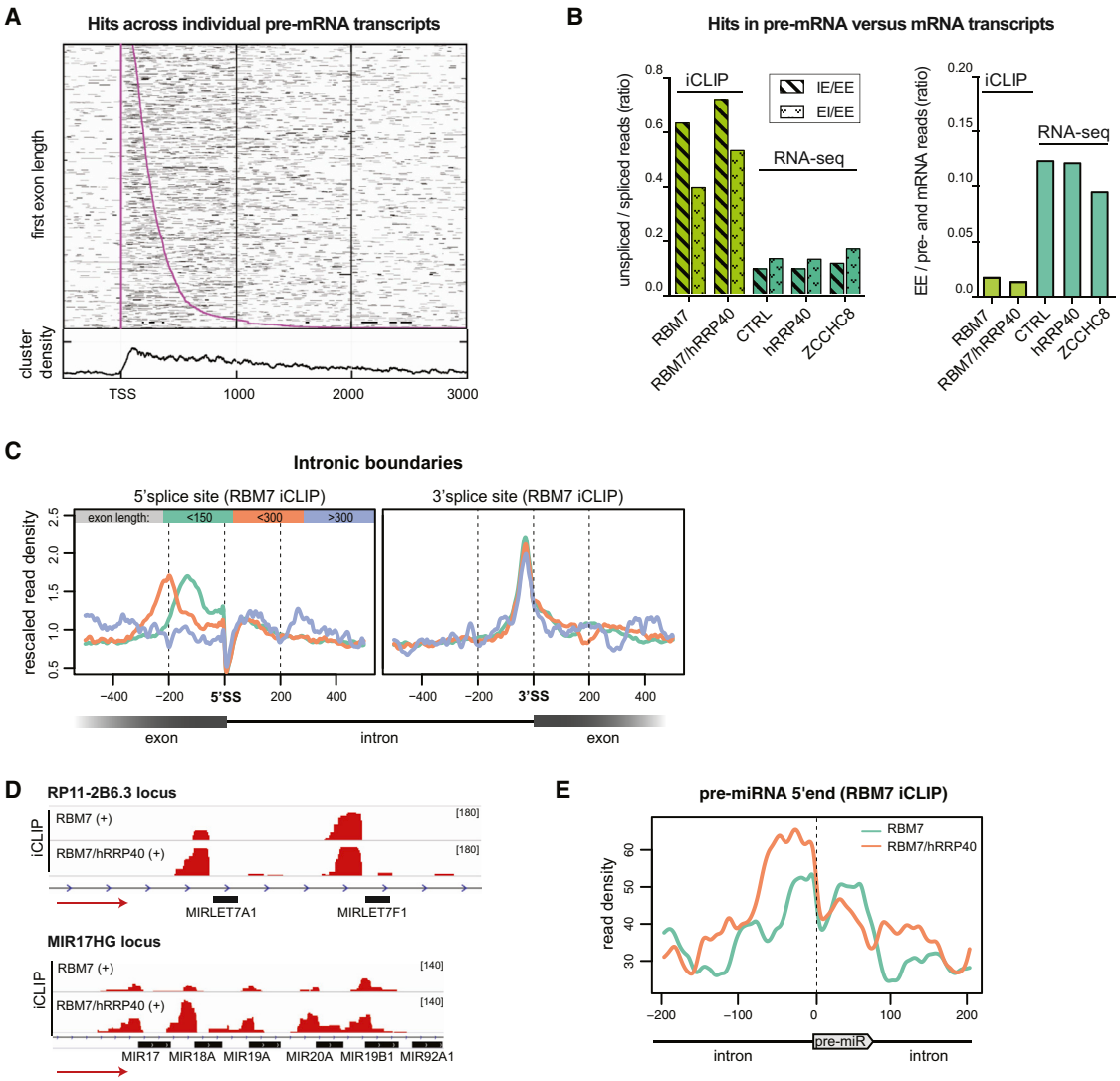

Figure 5. RBM7 Binds Pre-mRNA and Accumulates at Intronic 3′ Ends

(A) RBM7 iCLIP reads mapped along pre-mRNAs using their annotated 5′ ends as anchoring sites (vertical purple line). Displayed transcripts were ordered by ascending first exon length with the EI boundary colored purple. Read density over all analyzed RNAs is shown at the bottom.

(B) (Left) Bar plots showing the fraction of mRNA/pre-mRNA mappers of iCLIP and RNA-seq reads, from the indicated libraries, spanning IE or EI relative to EE junctions. (Right) Same as left, but displaying reads spanning EE relative to the sum of IE, EI, and EE junctions (average of the two iCLIP replicates).

(C) Density profiles of RBM7 iCLIP reads over a region spanning 0.5 kb upstream and downstream of EI (left) or IE (right) boundaries. Reads were assembled from nonterminal introns flanked by exons of different lengths as indicated by color coding.

(D) Genome browser screenshot of RBM7 iCLIP and RNA-seq reads mapped to representative introns encoding the indicated pre-miRNAs ((+) strand only). The nomenclature is as in Figure 1C.

(E) Density plots of iCLIP read clusters over regions spanning 0.5 kb upstream and downstream of pre-miRNA borders. The nomenclature is as in Figure 4E.

To examine the role of NEXT/exosome complexes in snoRNA metabolism, we depleted cells of either the core exosome subunit hRRP40 or one of its two catalytic subunits hRRP6 and hDIS3. Northern probes targeting the 3′-extended regions of SNORD83A, SNORD43, SNORA6, and SNORA62 revealed an accumulation of 3′-lengthened transcripts in all knockdown experiments (Figure 6C, top). hRRP40 depletion yielded the strongest phenotype, in line with the reported functional redundancy of hDIS3 and hRRP6 (Preker et al., 2008). Despite effective protein depletions (Figure S5E), we detected no major differences in levels of mature snoRNAs (Figure 6C, bottom). The interaction of RBM7 with 3′-extended snoRNAs was verified by employing the RBM7-RIP approach, combined with depletion of hRRP40. For all four tested RNAs, SNORD43, SNORD83A, SNORA73A, and SNORA73B, species corresponding to snoRNAs matured at their 5′ ends and extended at their 3′ ends, down to the host intronic 3′ SSs, were detected in a hRRP40 depletion-dependent manner (Figure 6D). IP of the

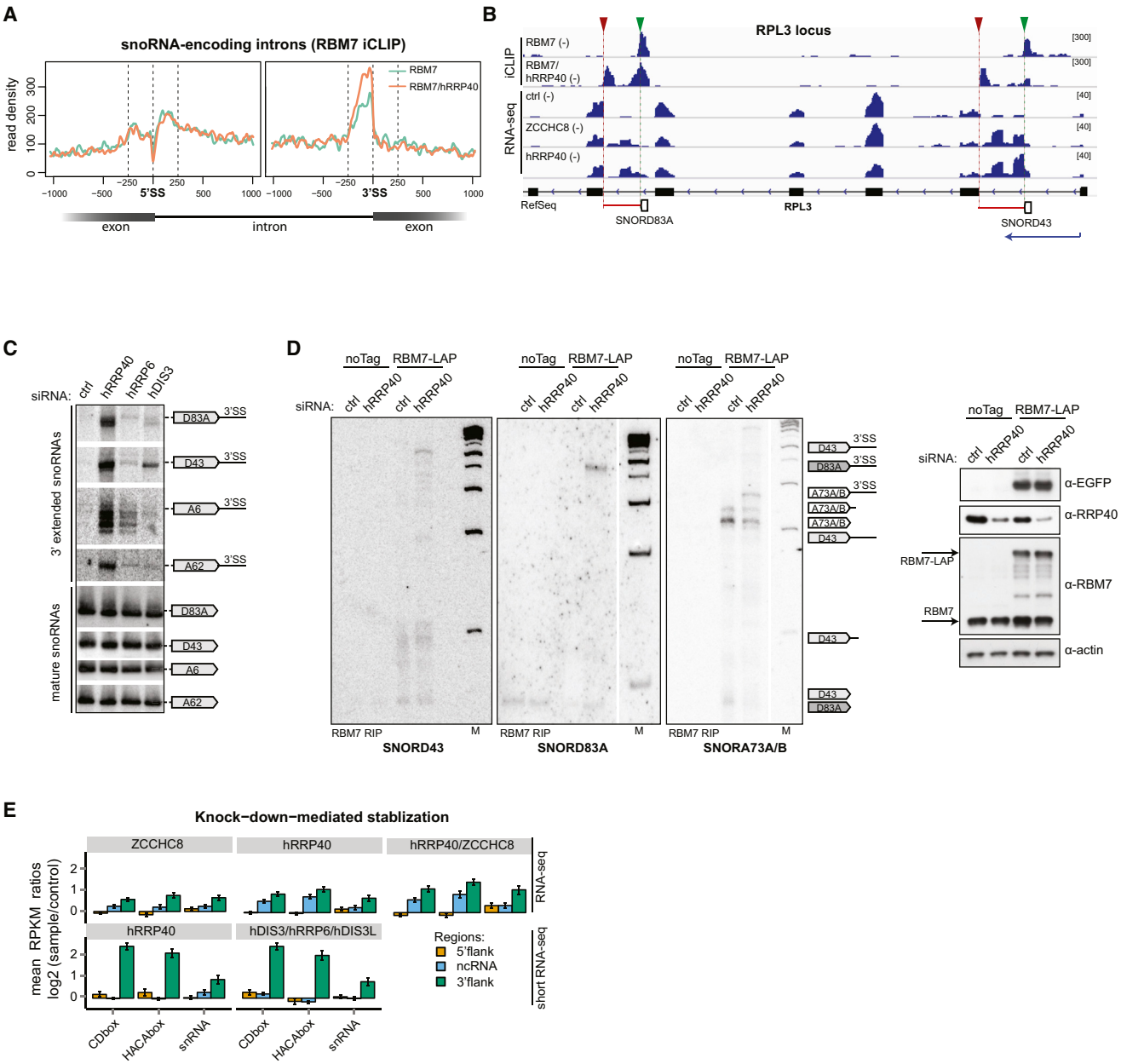

Figure 6. RBM7 Targets the RNA Exosome to SnoRNA-Encoding Introns

(A) Density profiles of RBM7 iCLIP reads from control and hRRP40-depleted libraries across snoRNA-encoding introns, plotted as in Figure 4C.

(B) Genome browser screenshot of RBM7 iCLIP and RNA-seq reads mapped to the RPL3 locus, hosting intronic snoRNAs ((−) strand only). Red arrows and bars indicate 3′ SSs and snoRNA 3′ extensions, respectively. Green arrow indicates the mature snoRNA 3′ end.

(C) Northern blotting analysis of total RNA from siRNA-depleted samples, as indicated. The top and bottom images show membranes probed against the 3′-extended and mature species of the noted snoRNAs, respectively. 3′ SS denotes the position of the 3′ SS of the snoRNA host intron.

(D) Northern blotting analysis (left) of RBM7-RIP'ed RNAs from control- or hRRP40-depleted samples. Both total (noTag) and RBM7-bound (RBM7-LAP) samples were probed against SNORD43, SNORD83A, and SNORA73A/B, as indicated. M, molecular weight markers. Western blotting analysis (right) of protein extracts from cells treated with siRNA against hRRP40 or luciferase (control). β-actin served as a loading control. Northern blots showing mature snoRNA levels of input samples are in Figure S5F.

(E) Global effects of exosome and NEXT complex component depletion on mature snoRNA/snRNA and their flanking regions. Standard RNA-seq (RNA-seq, top) and RNA-seq libraries targeting mature snoRNA and snRNA (short RNA-seq, bottom) were employed. Y axes show log(2)-scaled mean reads per 10 million mapped reads (RP10M) fold changes in the indicated samples relative to their GFP siRNA control. C/D- and H/ACA box intronic snoRNAs as well as all snRNAs are plotted with separate mean RP10M ratios for the mature ncRNA (blue), the upstream (orange), and downstream (green) flanking regions. 5′ and 3′ flanks of intronic snoRNA were taken as the respective intronic regions of the host intron. 5′ and 3′ flanks of snRNAs were the immediate upstream and downstream 500 bp of each gene.

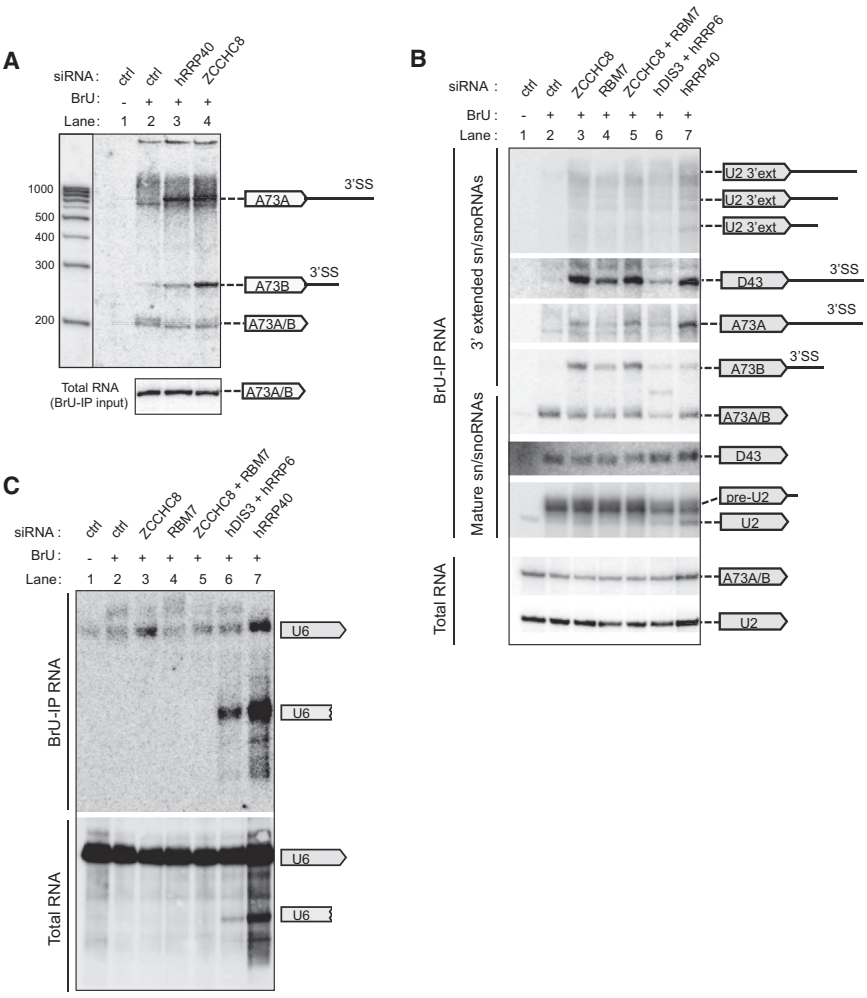

Figure 7. The NEXT Complex Targets Newly Synthesized RNA

(A) Northern blotting analysis of RNA BrU-labeled for 1 hr and BrU-IP'ed from cells depleted of the indicated proteins. Part of the corresponding Northern blot of BrU-IP input samples is also shown (bottom). Blots were hybridized with end-labeled oligonucleotide probes targeting the mature forms of SNORA73A/B.

(B and C) Northern blotting analyses performed and displayed as in (A) and annotated as in Figure 6C. All utilized northern probes targeted the indicated mature snRNA/snoRNA species.

mature snoRNA counterparts was subjected to some background and did not yield conclusive results (Figures 6D and S5F). Still, we suggest that RBM7 recruits the exosome to 3′-extended snoRNA transcripts and that exosome activity ensues subsequent to snoRNA 5′ processing.

Finally, we performed an RNA-seq-based quantification of human snoRNAs and snRNAs, including their flanking regions. As our original datasets were biased toward longer transcripts (>150 nt) and therefore did not detect most mature snoRNAs, we prepared libraries enriched for shorter species (<200 nt, called "short RNA-seq") from cells depleted of hRRP40 or all three catalytic subunits of the RNA exosome (hDIS3/hRRP6/hDIS3L). In the original RNA-seq libraries a pronounced increase in tags mapping to a region covering the gene body as well as the 3′ flanks of both the H/ACA and C/D box snoRNAs was evident upon single ZCCHC8 and hRRP40 depletions as well as in their combined depletion (Figure 6E, top). However, while fragments mapping to the 3′ flanks were also highly enriched in the short RNA-seq libraries, depletion of hRRP40 or codepletion of hDIS3, hDIS3L, and hRRP6 did not alter levels of mature snoRNAs and snRNAs (Figure 6E, bottom). Although this could indicate that the RNA exosome is not involved in intronic snoRNA biogenesis, we note that residual exosome complexes, long half-lives of mature snoRNA, and possible compensatory mechanisms that ensure stable snoRNA levels may mask such involvement (see below and Discussion). In any event, we conclude that targeting of NEXT/exosome to 3′-extended snoRNAs/snRNAs is general.

RBM7 Targets Newly Synthesized RNA

All analyses so far are compatible with early binding of RBM7 during RNA production. To directly assess whether NEXT acts at the level of newly synthesized RNA, we utilized Northern blotting analysis to monitor 3′-extended snoRNA transcript purified by 5-bromouridine (BrU)-IP. Following the efficient depletion of hRRP40 and ZCCHC8 (Figures S6A and S6B) and a 1-hour BrU labeling pulse, a strong accumulation of BrU-IP'ed 3′-extended SNORA73A and SNORA73B was apparent (Figure 7A, compare lanes 3 and 4 with lane 2). Depletions of hDIS3 and hRRP6 showed less accumulation probably because their codepletion was not highly efficient (Figures 7B and S6B). Interestingly, depletion of ZCCHC8 resulted in RNA levels comparable (3′-extended SNORA73A) or even higher (3′-extended SNORA73B) than after hRRP40 depletion. This is counter to the effects of these knockdowns on steady-state RNA levels (Andersen et al., 2013; Lubas et al., 2011) and may reflect a dedicated utility of NEXT at the level of newly synthesized RNA, whereas the exosome also employs a cofactor(s) that acts posttranscriptionally (see Discussion). An impact of RBM7 on newly synthesized RNA was directly revealed by extending the BrU-IP samples to include knockdowns of RBM7 and its combination with ZCCHC8. Assaying intronic snoRNAs and U2 snRNA showed that depletion of RBM7 led to the accumulation of BrU-labeled 3′-extended transcripts at an extent similar to depletion of ZCCHC8 and hRRP40 (Figures 7B and S6C–S6I).

We also probed for U6 snRNA and observed faster migrating species upon depletion of hDIS3+hRRP6 or hRRP40 (Figure 7C, top, lanes 6 and 7). These exosome substrates likely represent

U6 decay products that are present in the BrU-IPs due to TUTase-mediated incorporation of BrU at their 3′ ends (Trippe et al., 2006). Steady-state RNA analyses demonstrated that these intermediates represent a minor portion of the total U6 snRNA pool (Figure 7C, bottom). Importantly, however, neither individual depletion of ZCCHC8 or RBM7 nor their combined depletion allowed the detection of U6 decay intermediates. This suggests that NEXT is not involved in this, likely posttranscriptional, exosome targeting to U6 snRNA. In summary, the similar phenotypes of NEXT complex and RNA exosome inhibition at the level of BrU-labeled RNA further support the idea that the NEXT complex functions in specifying exosome substrates among newly synthesized transcripts.

DISCUSSION

The variety of substrates of the human nuclear exosome begs the question of how these different RNAs are targeted. As human Nrd1p/Nab3p homologs have not been reported, the exosome-interacting NEXT complex was suggested to play an important, yet not fully characterized, role in RNA binding and exosome recruitment (Andersen et al., 2013; Lubas et al., 2011). Indeed, the present iCLIP analysis of the NEXT component RBM7 is fully consistent with NEXT being a central cofactor of the nuclear exosome. In addition, it forwards our understanding of exosome-recruitment strategies in human nuclei considerably. Similar to Nrd1p and Nab3p deposition in *S. cerevisiae*, RBM7 is loaded early onto RNA. However, in contrast to the Nrd1p/Nab3 system, RBM7 binding to target transcripts appears to occur without strong sequence specificity, showing some preference for U-rich sequences, the functional relevance of which remains to be investigated. We demonstrate that such promiscuous RBM7 binding, if combined with an available nearby RNA 3′ end, provides the sufficient in-road for exosome targeting of several nuclear transcript classes.

RBM7 Marks Newly Synthesized RNA for Exosome Degradation

Our data illustrate several examples of physical interactions between RBM7 and known nuclear substrates of the RNA exosome. The enrichment of RBM7 is pronounced in proximity to cellular TSSs that direct the synthesis of PROMPTs and eRNAs, transcript species that also accumulate upon depletion of the NEXT components ZCCHC8 and hMTR4 as well as exosome core components (Figures 2 and 3). The binding of RBM7 to intron-less lncRNA and the increase in RBM7 iCLIP signal upon hRRP40 depletion (Figure 3D) further add to the suggestion that NEXT recruits the exosome to degrade RNA. RBM7 is also found associated with relatively short and exosome-sensitive 3′-extended RNAs arising from snRNA and RDH genes (Andersen et al., 2013). RBM7 binding is detected in the mature snRNAs, but considering their much higher abundance, this interaction is likely taking place very transiently or to a minor pool of the total mature snRNA. Altogether, the data clearly confirm that the investigated prominent classes of exosome substrates in human nuclei all associate with RBM7.

In addition to its binding to PROMPTs, RBM7 also associates with RNAs transcribed in the sense direction of genic TSSs. A part of the TSS-proximal signal presumably originates from RBM7-association with short ~100–1,000 nt RNAs derived from promoter-proximal transcription termination events (Ntini et al., 2013) and constituting substrates of the exosome. In *S. cerevisiae*, Mtr4p was reported to bind to similar promoter-proximal sense transcripts (Tuck and Tollervey, 2013). Whether this reflects a conserved difficulty for RNAPII to achieve sufficient elongation capacity during the first hundred base pairs of transcription from the TSS or whether the production of such promoter-proximal RNAs is part of a conserved regulatory mechanism remains to be elucidated. For now we suggest that these human RNAs are targeted by the exosome via their deposited RBM7 protein.

Given that splicing is often cotranscriptional (Brugiolo et al., 2013), the proposed targeting of newly synthesized RNA by RBM7 is further revealed by its preferential association with pre-mRNA relative to mRNA (Figures 5A and 5B). Furthermore, the general binding of RBM7 along pre-mRNAs with a clear enrichment for the cap-proximal ~1,000 nts (Figure 5A) highlights a couple of interesting features of RBM7 biology. First, the presence of RBM7 on RNA does not inevitably result in exosome degradation. Instead, it appears that RBM7 associates rather generally with RNA and only if a 3′ end becomes available in the vicinity will 3′-5′ exonucleolysis by the exosome follow. PROMPTs, eRNAs, and 3′-extended RNAs represent nuclear exosome targets where RBM7 association, NEXT assembly, and the occurrence of a naked 3′ end is happening within a short time frame. Second, the enrichment of RBM7 at 5′ ends of pre-mRNA and our RBM7 RIP experiment combined with CBC depletion (Figure 2C) suggests that one contribution to recruiting the protein to early RNAPII-transcripts is via its interaction with the CBC (Andersen et al., 2013; Lubas et al., 2011). An early recruitment of RBM7 is further supported by its recently reported localization in both chromatin and nucleoplasmic cell fractions (Blasius et al., 2014). In other cases, as exemplified by intron binding, RBM7/NEXT could also intersect with other RNA processing events, such as splicing.

The NEXT Complex Targets 3′-Extended snoRNAs

RBM7 occupies introns, particularly at their 3′ ends. Most prominently, upon exosome/NEXT depletion, snoRNA-hosting introns display a marked stabilization of, and an increased RBM7 binding to, the 3′-intronic region flanking the snoRNA (Figure 6). In these cases, full intron decay by XRN2 is likely blocked by structures of early-formed pre-snoRNPs (Richard et al., 2006). This implies that 5′ and 3′ end snoRNA processing/decay operate independently. It also underscores a role of NEXT in targeting the exosome to these 3′-extended substrates. Given that mature snoRNA levels are orders of magnitudes higher than their 3′-extended counterparts, RBM7 must bind the latter with high affinity, directly involving NEXT complex function in the metabolism of these transcripts.

We find that depletion of exosome/NEXT components does not markedly affect steady state levels of mature snoRNA (Figures 6C and 6E) and only to some extent in BrU-IP'ed samples (Figure 7C). This could suggest that the RNA exosome does not play a major role in the biogenesis of human intronic snoRNA. However, because of the long half-lives of mature snoRNA and

possible redundant processing pathways, further investigations are needed. While the observed NEXT-mediated exosome targeting of 3′-extended snoRNAs may result in the production of mature species, it is also possible that NEXT facilitates their complete degradation. A conceptually similar observation was reported for tRNA precursors in *S. cerevisiae* (Gudipati et al., 2012). In this way, the complete turnover of apparent precursor molecules may either represent a mechanism of snoRNP quality control, in which improperly assembled snoRNP particles are degraded, or the simple removal of "surplus" ncRNA material.

Temporal Separation of Human Nuclear RNA Decay Pathways

Strikingly, our metabolic labeling experiments revealed an accumulation of 3′-extended newly synthesized snoRNA species in cells depleted of ZCCHC8, RBM7, and hRRP40 (Figures 7A and 7B). In contrast, steady-state analysis of snoRNAs (Figure 6E) and other exosome substrates (Andersen et al., 2013; Lubas et al., 2011) results in less pronounced phenotypes upon NEXT depletion compared with RRP40-depletion. This supports our model that NEXT specifies early exosome substrates like PROMPTs, eRNAs, and 3′-extended snoRNAs. It also argues that other exosome-dependent decay pathway(s) may take over in the absence of NEXT or when NEXT is saturated. One such pathway is specified by the nuclear poly(A)-binding protein, PABPN1, which functionally connects the RNA exosome to substrates that are already spliced and polyadenylated (Beaulieu et al., 2012). This, and other possible nuclear turnover pathways, likely constitute separate, but complementary check points, enabling continued RNA quality control en route from RNA transcription to nuclear export. A major future challenge will be to decompose specific transcript half-lives into their different kinetic components and turnover mechanisms.

EXPERIMENTAL PROCEDURES

A more detailed description of the Materials and Methods is provided in the Supplemental Experimental Procedures.

Cell Culture and RNAi

HeLa cells were seeded in Dulbecco's modified Eagle's medium and transfected using Lipofectamine 2000 (Invitrogen) and siRNA at a final concentration of 15 nM. Knockdown efficiency was validated by western blotting and RNA isolated for analyses using TRIzol (Life Technologies).

RNA Abundance Analyses

The abundance of individual transcripts was measured in RNA samples either by Northern blotting analysis, using standard protocol or globally by RNA-seq. RNA libraries were prepared using rRNA-depleted total RNA (Ribozero, Epicenter) and the NEBNext Small RNA Library Kit (NEB). For detection of newly synthesized RNA, metabolic labeling and purification of newly synthesized transcripts were done as described in (Paulsen et al., 2013) with modifications described in the Supplemental Experimental Procedures.

iCLIP and RBM7-RIP

iCLIP and RBM7-RIP experiments were performed using HeLa cells stably expressing a C-terminally LAP-tagged RBM7 variant, including a GFP moiety. Cells were irradiated with UV light at 254 nm, and purification of RBM7-bound RNA was done as described in the original iCLIP protocol (König et al., 2010) with modifications noted in the Supplemental Experimental Procedures.

ACCESSION NUMBERS

The data associated with the manuscript have been deposited to the NCBI Gene Expression Omnibus and are available under accession numbers GSE63791 (iCLIP) and GSE63496 (short RNA-seq). The previously published RNA-seq, CAGE, and 3′ TAG datasets used in this study were downloaded from accession numbers GSE52132 and GSE48286.

SUPPLEMENTAL INFORMATION

Supplemental Information includes Supplemental Experimental Procedures and six figures and can be found with this article online at http://dx.doi.org/10.1016/j.celrep.2014.12.026.

AUTHOR CONTRIBUTIONS

M.L., P.R.A., and T.H.J. designed and interpreted experiments and wrote the manuscript. M.L., P.R.A., and A.S. performed experiments. M.L., P.R.A., and G.K. analyzed sequencing data. A.D. supervised M.L. and aided with data interpretation.

ACKNOWLEDGMENTS

We thank Joanna Kufel, Edouard Bertrand, Søren Lykke-Andersen, and Christian K. Damgaard for critical comments on the manuscript; Dorthe C. Riishøj and Claudia Scheffler for technical assistance; and Robin Andersson and Thomas Hansen for help with RNA annotations. This work was supported by the Danish National Research Foundation (grant DNRF58), the Danish Cancer Society and the Lundbeck and Novo Nordisk Foundations (to T.H.J.), the Polish National Science Center (2011/02/A/NZ1/00001 Maestor grant to A.D.) and the Welcome Trust (grant 097383) and the Medical Research Council (to G.K.). M.L. was supported by a Boehringer-Ingelheim PhD fellowship and a START fellowship from the Foundation for Polish Science.

Received: June 24, 2014
Revised: October 29, 2014
Accepted: December 11, 2014
Published: January 8, 2015

REFERENCES

Anamika, K., Gyenis, À., Poidevin, L., Poch, O., and Tora, L. (2012). RNA polymerase II pausing downstream of core histone genes is different from genes producing polyadenylated transcripts. PLoS ONE *7*, e38769.

Andersen, P.R., Domanski, M., Kristiansen, M.S., Storvall, H., Ntini, E., Verheggen, C., Schein, A., Bunkenborg, J., Poser, I., Hallais, M., et al. (2013). The human cap-binding complex is functionally connected to the nuclear RNA exosome. Nat. Struct. Mol. Biol. *20*, 1367–1376.

Andersson, R., Andersen, P.R., Valen, E., Core, L., Bornholdt, J., Boyd, M., Jensen, T.H., and Sandelin, A. (2014a). Nuclear stability and transcriptional directionality separate functionally distinct RNA species. Nat. Commun. *5*, 5336.

Andersson, R., Gebhard, C., Miguel-Escalada, I., Hoof, I., Bornholdt, J., Boyd, M., Chen, Y., Zhao, X., Schmidl, C., Suzuki, T., et al.; FANTOM Consortium (2014b). An atlas of active enhancers across human cell types and tissues. Nature *507*, 455–461.

Änkö, M.L., Müller-McNicoll, M., Brandl, H., Curk, T., Gorup, C., Henry, I., Ule, J., and Neugebauer, K.M. (2012). The RNA-binding landscapes of two SR proteins reveal unique functions and binding to diverse RNA classes. Genome Biol. *13*, R17.

Arigo, J.T., Eyler, D.E., Carroll, K.L., and Corden, J.L. (2006). Termination of cryptic unstable transcripts is directed by yeast RNA-binding proteins Nrd1 and Nab3. Mol. Cell *23*, 841–851.

Beaulieu, Y.B., Kleinman, C.L., Landry-Voyer, A.M., Majewski, J., and Bachand, F. (2012). Polyadenylation-dependent control of long noncoding RNA expression by the poly(A)-binding protein nuclear 1. PLoS Genet. *8*, e1003078.

Berndt, H., Harnisch, C., Rammelt, C., Stöhr, N., Zirkel, A., Dohm, J.C., Himmelbauer, H., Tavanez, J.P., Hüttelmaier, S., and Wahle, E. (2012). Maturation of mammalian H/ACA box snoRNAs: PAPD5-dependent adenylation and PARN-dependent trimming. RNA *18*, 958–972.

Blasius, M., Wagner, S.A., Choudhary, C., Bartek, J., and Jackson, S.P. (2014). A quantitative 14-3-3 interaction screen connects the nuclear exosome targeting complex to the DNA damage response. Genes Dev. *28*, 1977–1982.

Brugiolo, M., Herzel, L., and Neugebauer, K.M. (2013). Counting on co-transcriptional splicing. F1000Prime Rep. *5*, 9.

Carroll, K.L., Ghirlando, R., Ames, J.M., and Corden, J.L. (2007). Interaction of yeast RNA-binding proteins Nrd1 and Nab3 with RNA polymerase II terminator elements. RNA *13*, 361–373.

Chlebowski, A., Lubas, M., Jensen, T.H., and Dziembowski, A. (2013). RNA decay machines: the exosome. Biochim. Biophys. Acta *1829*, 552–560.

Cuello, P., Boyd, D.C., Dye, M.J., Proudfoot, N.J., and Murphy, S. (1999). Transcription of the human U2 snRNA genes continues beyond the 3′ box in vivo. EMBO J. *18*, 2867–2877.

De Santa, F., Barozzi, I., Mietton, F., Ghisletti, S., Polletti, S., Tusi, B.K., Muller, H., Ragoussis, J., Wei, C.L., and Natoli, G. (2010). A large fraction of extragenic RNA pol II transcription sites overlap enhancers. PLoS Biol. *8*, e1000384.

Fasken, M.B., Leung, S.W., Banerjee, A., Kodani, M.O., Chavez, R., Bowman, E.A., Purohit, M.K., Rubinson, M.E., Rubinson, E.H., and Corbett, A.H. (2011). Air1 zinc knuckles 4 and 5 and a conserved IWRXY motif are critical for the function and integrity of the Trf4/5-Air1/2-Mtr4 polyadenylation (TRAMP) RNA quality control complex. J. Biol. Chem. *286*, 37429–37445.

Gruber, J.J., Zatechka, D.S., Sabin, L.R., Yong, J., Lum, J.J., Kong, M., Zong, W.X., Zhang, Z., Lau, C.K., Rawlings, J., et al. (2009). Ars2 links the nuclear cap-binding complex to RNA interference and cell proliferation. Cell *138*, 328–339.

Gudipati, R.K., Xu, Z., Lebreton, A., Séraphin, B., Steinmetz, L.M., Jacquier, A., and Libri, D. (2012). Extensive degradation of RNA precursors by the exosome in wild-type cells. Mol. Cell *48*, 409–421.

Hallais, M., Pontvianne, F., Andersen, P.R., Clerici, M., Lener, D., Benbahouche, Nel.H., Gostan, T., Vandermoere, F., Robert, M.C., Cusack, S., et al. (2013). CBC-ARS2 stimulates 3′-end maturation of multiple RNA families and favors cap-proximal processing. Nat. Struct. Mol. Biol. *20*, 1358–1366.

Hirose, T., Shu, M.D., and Steitz, J.A. (2003). Splicing-dependent and -independent modes of assembly for intron-encoded box C/D snoRNPs in mammalian cells. Mol. Cell *12*, 113–123.

Kim, T.K., Hemberg, M., Gray, J.M., Costa, A.M., Bear, D.M., Wu, J., Harmin, D.A., Laptewicz, M., Barbara-Haley, K., Kuersten, S., et al. (2010). Widespread transcription at neuronal activity-regulated enhancers. Nature *465*, 182–187.

Kiss, T., and Filipowicz, W. (1995). Exonucleolytic processing of small nucleolar RNAs from pre-mRNA introns. Genes Dev. *9*, 1411–1424.

König, J., Zarnack, K., Rot, G., Curk, T., Kayikci, M., Zupan, B., Turner, D.J., Luscombe, N.M., and Ule, J. (2010). iCLIP reveals the function of hnRNP particles in splicing at individual nucleotide resolution. Nat. Struct. Mol. Biol. *17*, 909–915.

Konig, J., Zarnack, K., Rot, G., Curk, T., Kayikci, M., Zupan, B., Turner, D.J., Luscombe, N.M., and Ule, J. (2011). iCLIP—transcriptome-wide mapping of protein-RNA interactions with individual nucleotide resolution. J. Vis. Exp.

LaCava, J., Houseley, J., Saveanu, C., Petfalski, E., Thompson, E., Jacquier, A., and Tollervey, D. (2005). RNA degradation by the exosome is promoted by a nuclear polyadenylation complex. Cell *121*, 713–724.

Lubas, M., Christensen, M.S., Kristiansen, M.S., Domanski, M., Falkenby, L.G., Lykke-Andersen, S., Andersen, J.S., Dziembowski, A., and Jensen, T.H. (2011). Interaction profiling identifies the human nuclear exosome targeting complex. Mol. Cell *43*, 624–637.

Morlando, M., Ballarino, M., Gromak, N., Pagano, F., Bozzoni, I., and Proudfoot, N.J. (2008). Primary microRNA transcripts are processed co-transcriptionally. Nat. Struct. Mol. Biol. *15*, 902–909.

Ntini, E., Järvelin, A.I., Bornholdt, J., Chen, Y., Boyd, M., Jørgensen, M., Andersson, R., Hoof, I., Schein, A., Andersen, P.R., et al. (2013). Polyadenylation site-induced decay of upstream transcripts enforces promoter directionality. Nat. Struct. Mol. Biol. *20*, 923–928.

Paulsen, M.T., Veloso, A., Prasad, J., Bedi, K., Ljungman, E.A., Tsan, Y.C., Chang, C.W., Tarrier, B., Washburn, J.G., Lyons, R., et al. (2013). Coordinated regulation of synthesis and stability of RNA during the acute TNF-induced proinflammatory response. Proc. Natl. Acad. Sci. USA *110*, 2240–2245.

Preker, P., Nielsen, J., Kammler, S., Lykke-Andersen, S., Christensen, M.S., Mapendano, C.K., Schierup, M.H., and Jensen, T.H. (2008). RNA exosome depletion reveals transcription upstream of active human promoters. Science *322*, 1851–1854.

Preker, P., Almvig, K., Christensen, M.S., Valen, E., Mapendano, C.K., Sandelin, A., and Jensen, T.H. (2011). PROMoter uPstream Transcripts share characteristics with mRNAs and are produced upstream of all three major types of mammalian promoters. Nucleic Acids Res. *39*, 7179–7193.

Reis, C.C., and Campbell, J.L. (2007). Contribution of Trf4/5 and the nuclear exosome to genome stability through regulation of histone mRNA levels in Saccharomyces cerevisiae. Genetics *175*, 993–1010.

Richard, P., Kiss, A.M., Darzacq, X., and Kiss, T. (2006). Cotranscriptional recognition of human intronic box H/ACA snoRNAs occurs in a splicing-independent manner. Mol. Cell. Biol. *26*, 2540–2549.

Rogelj, B., Easton, L.E., Bogu, G.K., Stanton, L.W., Rot, G., Curk, T., Zupan, B., Sugimoto, Y., Modic, M., Haberman, N., et al. (2012). Widespread binding of FUS along nascent RNA regulates alternative splicing in the brain. Sci Rep *2*, 603.

Schneider, C., and Tollervey, D. (2013). Threading the barrel of the RNA exosome. Trends Biochem. Sci. *38*, 485–493.

Schneider, C., Kudla, G., Wlotzka, W., Tuck, A., and Tollervey, D. (2012). Transcriptome-wide analysis of exosome targets. Mol. Cell *48*, 422–433.

Shcherbik, N., Wang, M., Lapik, Y.R., Srivastava, L., and Pestov, D.G. (2010). Polyadenylation and degradation of incomplete RNA polymerase I transcripts in mammalian cells. EMBO Rep. *11*, 106–111.

Sloan, K.E., Schneider, C., and Watkins, N.J. (2012). Comparison of the yeast and human nuclear exosome complexes. Biochem. Soc. Trans. *40*, 850–855.

Steinmetz, E.J., Conrad, N.K., Brow, D.A., and Corden, J.L. (2001). RNA-binding protein Nrd1 directs poly(A)-independent 3′-end formation of RNA polymerase II transcripts. Nature *413*, 327–331.

Sugimoto, Y., König, J., Hussain, S., Zupan, B., Curk, T., Frye, M., and Ule, J. (2012). Analysis of CLIP and iCLIP methods for nucleotide-resolution studies of protein-RNA interactions. Genome Biol. *13*, R67.

Thiebaut, M., Kisseleva-Romanova, E., Rougemaille, M., Boulay, J., and Libri, D. (2006). Transcription termination and nuclear degradation of cryptic unstable transcripts: a role for the nrd1-nab3 pathway in genome surveillance. Mol. Cell *23*, 853–864.

Trippe, R., Guschina, E., Hossbach, M., Urlaub, H., Lührmann, R., and Benecke, B.J. (2006). Identification, cloning, and functional analysis of the human U6 snRNA-specific terminal uridylyl transferase. RNA *12*, 1494–1504.

Tuck, A.C., and Tollervey, D. (2013). A transcriptome-wide atlas of RNP composition reveals diverse classes of mRNAs and lncRNAs. Cell *154*, 996–1009.

Tudek, A., Porrua, O., Kabzinski, T., Lidschreiber, M., Kubicek, K., Fortova, A., Lacroute, F., Vanacova, S., Cramer, P., Stefl, R., and Libri, D. (2014). Molecular basis for coordinating transcription termination with noncoding RNA degradation. Mol. Cell *55*, 467–481.

Valen, E., Preker, P., Andersen, P.R., Zhao, X., Chen, Y., Ender, C., Dueck, A., Meister, G., Sandelin, A., and Jensen, T.H. (2011). Biogenic mechanisms and utilization of small RNAs derived from human protein-coding genes. Nat. Struct. Mol. Biol. *18*, 1075–1082.

Vanácová, S., Wolf, J., Martin, G., Blank, D., Dettwiler, S., Friedlein, A., Langen, H., Keith, G., and Keller, W. (2005). A new yeast poly(A) polymerase complex involved in RNA quality control. PLoS Biol. *3*, e189.

Vasiljeva, L., and Buratowski, S. (2006). Nrd1 interacts with the nuclear exosome for 3′ processing of RNA polymerase II transcripts. Mol. Cell *21*, 239–248.

Wlotzka, W., Kudla, G., Granneman, S., and Tollervey, D. (2011). The nuclear RNA polymerase II surveillance system targets polymerase III transcripts. EMBO J. *30*, 1790–1803.

Wolin, S.L., Sim, S., and Chen, X. (2012). Nuclear noncoding RNA surveillance: is the end in sight? Trends Genet. *28*, 306–313.

Wyers, F., Rougemaille, M., Badis, G., Rousselle, J.C., Dufour, M.E., Boulay, J., Régnault, B., Devaux, F., Namane, A., Séraphin, B., et al. (2005). Cryptic pol II transcripts are degraded by a nuclear quality control pathway involving a new poly(A) polymerase. Cell *121*, 725–737.

Zarnack, K., König, J., Tajnik, M., Martincorena, I., Eustermann, S., Stévant, I., Reyes, A., Anders, S., Luscombe, N.M., and Ule, J. (2013). Direct competition between hnRNP C and U2AF65 protects the transcriptome from the exonization of Alu elements. Cell *152*, 453–466.

Zünd, D., Gruber, A.R., Zavolan, M., and Mühlemann, O. (2013). Translation-dependent displacement of UPF1 from coding sequences causes its enrichment in 3′ UTRs. Nat. Struct. Mol. Biol. *20*, 936–943.